LAPP (IN2P3)

LABORATOIRE D'ANNECY-LE-VIEUX DE PHYSIQUE
DES PARTICULES

BOITE POSTALE 909 74019 ANNECY-LE-VIEUX CÉDEX, FRANCE

LAPP -- 80-05.

MULTIMUON FINAL STATES

José-Maria CRESPO

Talk given at the "VIIIth International Winter Meeting on fundamental physics", RONDA (SPAIN), March 24-29 1980.

LAPP -80-05
APRIL 1980

Abstract.

Multimuon final states have been detected by 3 experiments in the interactions of the muon beams of Cern (280GeV) and FNAL (210 GeV) with heavy targets. For the first time production of J/ψ (3100) by space-like photons has been observed and its dependence on ν, Q^2 and t compared to Vector Dominance and photon-gluon fusion models. Also a clear signal has been seen for 3μ above QED tridents (outside J/ψ mass range) and 2μ events which are well described by charm production. An upper limit for the production of the T by high energy muons has been set.

1. INTRODUCTION AND DEFINITIONS.

We report here the results on multimuon final states of three muon-nucleon scattering experiments. For all three, these results are based only on a fraction of $\sim$ 20 % of their data. Two of them are being performed in the CERN M2 beam line and the data reported here correspond to 280 GeV incident μ^+. These are experiments NA2 by the CERN-Desy-Freiburg-Kiel-Lancaster-LAPP-Liverpool-Oxford-Rutherford-Sheffield-Turin-Wuppertal or European Muon Collaboration (EMC) and NA4 by the Bologna-CERN-Dubna-Munich-Saclay Collaboration (BCDMS). The third experiment used the FNAL muon beam with 209 GeV μ^+ for the data reported here. This is the Berkeley-FNAL-Princeton Collaboration (BFP). Table I summarizes the main characteristics of these experiments.

We see that for NA2 and BFP the targets, made of iron and scintillators, are also calorimeters. By selecting events where the interaction takes place in the upstream part of the target, the hadrons remain in the target and their energy can be measured.

A description of the experimental set-ups can be found in other contributions to this conference for NA2 and NA4 experiments (1,2). For the BFP experiment (3) a very important feature for multimuon detection is the fact that, due to the lower intensity of the FNAL muon beam, all the chambers are fully sensitive in the beam region allowing the detection of the scattered muon which in most of multimuons events comes out at very low angles.

For NA4, the beam hole in the spectrometer is partly filled by the use of an end detector downstream the spectrometer. For NA2 the spectrometer is completed by proportional chambers and hodoscopes inside the beam allowing for detection but not momentum determination. This means that for (3 μ) events where the muons are labelled 0 for incoming, 1 for scattered, 2 and 3 for decay ones (fig.1) the experiments will be able to measure :

-BFP : all three momenta and angles.

-BCDMS : momenta and angles for 2 muons : p_2,θ_2, p_3,θ_3 and in $\sim$ 11 % of events also p_1,θ_1 with the end detector.

-EMC : momenta and angles for 2 muons : p_2,θ_2, p_3,θ_3 and in $\sim$ 70 % of events also θ_1 with the detectors in the beam. Then p_1 is calculated by energy balance :

$E_1 = E_0 + M_{nucleon} - E_2 - E_3 - E_{hadronic\ deposited}$.

Let us now define some kinematic quantities.

a) Usual deep inelastic variables (fig.2a).

Virtual photon energy :

$$\nu = E_0 - E_1 \text{ and momentum : } \vec{p}_\gamma = \vec{p}_0 - \vec{p}_1$$

Virtual photon squared mass :

$$q^2 = (E_0 - E_1)^2 - (\vec{p}_0 - \vec{p}_1)^2 \text{ and } Q^2 = -q^2$$

Hadronic system invariant mass squared :

$$W^2 = M_N^2 + 2M_N\nu - Q^2$$

b) Variables for 3μ events (fig. 2b).

The index (23) refers to the J/ψ or the μ_2,μ_3 system. Fraction of the photon energy taken by J/ψ or $(\mu^+\mu^-)$ pair : $Z = \frac{E_{23}}{\nu}$. Squared 4-momentum transfer from virtual photon to J/ψ or to $(\mu^+\mu^-)$ pair :

$$t = -[(\nu - E_{23})^2 - (\vec{p}_\gamma - \vec{p}_{23})^2]$$

where t is defined positive.

In practice, what one measures for t is the missing transverse momentum squared : $t \sim p^2_{\perp(missing)} = (\vec{p}_{1\perp} + \vec{p}_{2\perp} + \vec{p}_{3\perp})^2$.

One also defines the $p_\perp$ of the $(\mu^+\mu^-)$ pair relative to the virtual photon :

$$\vec{p}_\perp = \vec{p}_{23} - (\vec{p}_{23}.\vec{p}_\gamma)\frac{\vec{p}_\gamma}{|\vec{p}_\gamma|}$$

c) Variables for 2μ events (fig.2c).

Now Z and $p_\perp$ will refer to the only produced secondary

muon :

$$z = \frac{E_2}{\nu} \qquad \vec{p}_1 = \vec{p}_2 - (\vec{p}_2 . \vec{p}_\gamma) \frac{\vec{p}_\gamma}{|\vec{p}_\gamma|}$$

2. SOURCES OF MULTIMUON EVENTS.

The multimuon events observed in these experiments can come from several sources that we classify either as background if the production mechanism is already well known or as interesting processes if this is not the case. A third category will include those processes which are also very interesting but which cannot be clearly observed in these experiments.

a) Backgrounds.

The main contribution comes from electromagnetic tridents which include Bethe-Heither (2 examples of these in fig.3a) and Compton terms. Since the interaction is purely electromagnetic, they can be accurately estimated. This process will give mainly low invariant masses for the muon pairs.

Another source is decay into a muon of pions or kaons produced in the hadron vertex (fig.3b). These decay muons are mainly at low momentum.

We will also consider as background the vector meson production (fig.3c) when the vector meson is lighter than the J/ψ ($\rho, \omega, \phi, \rho'$, etc..). This contribution will be small due to the low branching ratio of the $\mu^+\mu^-$ decay mode.

b) Interesting processes.

The J/ψ production (fig.4a) can be detected by the J/ψ decay into ($\mu^+\mu^-$). Also the production of a $c\bar{c}$ pair (fig.4b) giving charmed particles can be seen through their muon decays. These two processes, hidden and open charm production, will be the main subject which the multimuon sample will allow to study. Table 2 gives in more detail the topics covered by each experiment. Published results are underlined.

c) Interesting but not (very much) seen processes.

Other very attractive sources of multimuons could be :

$\tau^+\tau^-$ production (fig.5a) as a new type of electromagnetic tridents, strongly suppressed however by the high propagator masses ; $b\bar{b}$ production (fig.5b) by photon-gluon fusion as seen for $c\bar{c}$; Drell-Yan pairs (fig.5c) by the photon acting as a $(q\bar{q})$ state ; production of a hypothetical heavy lepton either neutral M° or double charged M^{++} (fig.5d) by weak interaction of the incoming muon. For these processes, the reported experiments will only be able to set upper limits.

3. GENERAL RESULTS.

The invariant mass $M_{\mu^+\mu^-}$ plots are shown in fig.6-8 without acceptance corrections. In $(\mu^+\mu^+\mu^-)$ events the scattered μ^+ is taken to be either the more energetic (EMC) or the one with the smallest angle except if one muon has a momentum more than twice the other in which case the more energetic is taken (BFP). Both algorithms give negligible errors as applied in the respective experimental conditions. The applied algorithm will also be included in Monte Carlo simulations of both experiments.

Both the plots of BFP (fig.8) and EMC (fig.7) show clearly a peak at the J/ψ mass containing $\sim$ 1700 events and $\sim$ 300 events respectively. In the BCDMS plot (fig.6) this peak is at the same time an acceptance effect. This last plot extends up to higher values of $M_{\mu^+\mu^-}$ allowing a determination of an upper limit for Υ production.

4. J/ψ PRODUCTION.

The total cross-section as published by BFP is $\sigma(\mu Fe \rightarrow \mu\psi X) = 0.76 \pm 0.22$ nb/nucleon and after corrections for nuclear effects $\sigma(\mu N \rightarrow \mu\psi X) = 0.67 \pm 0.20$ nb. The unpublished results of EMC and BCDMS are in agreement with this.

a) Elastic production.

Results on elastic J/ψ production have been published both by BFP (4) and EMC (5). Elastic events are defined as those with a hadronic energy < 5 GeV deposited in the target

calorimeter. With this separation one gets rid of the cascade process $\mu N \rightarrow \mu\psi' X$

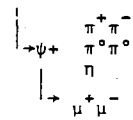

which, since only the final muons are detected, will appear as inelastic ψ production. In addition to the hadronic energy cut, the elastic samples have been corrected for radiative effects.

Shown in fig.9 is the $t' = t - t_{min}$ distribution of EMC and in fig.10 the corresponding one of BFP. Coherent and incoherent contributions for production on nucleus or on nucleon can easily be distinguished, although the slope of the coherent part is dominated by resolution of the apparatus. The distribution can be fitted to :

$$\frac{d\sigma}{dt})^{Fe} = [A_{eff}^2 \; e^{-at} + A_{eff} \; f(t)] \frac{d\sigma}{dt})^{nucleon}_{t=o}$$

where are takes :

BFP : $A_{eff} = 0.9 * A$ (for shadowing) ; $a = 150$ GeV^{-2}

EMC : $A_{eff} = A = 56$ (no shadowing taken into account) ; $a = 135$ GeV^{-2}

As already said, a remains unresolved and its value is deduced from previous photoproduction experiments on Berillium (ref.6). Then $f(t)$ is fitted to :

BFP : $f(t) = \frac{7}{8} e^{-3t} + \frac{1}{8} e^{-t}$ with $\chi^2 = 5.9/6$ DOF

EMC : $f(t) = e^{-bt}$ with $b = 2.31 \pm 0.30$ GeV^{-2}

The Q^2 dependence is shown in fig.11-12 for EMC and BFP and compared to the vector dominance model prediction $(1+\frac{Q^2}{M^2})^{-2}$. $M^2 = M_\rho^2$ and $M^2 = 1$ GeV^2 are ruled out whereas the best fit to the VDM form gives $M = 2.4 \pm 0.3$ GeV (EMC) and $M = 2.7 \pm 0.5$ GeV (BFP) compatible with $M = M_{J/\psi}$

In this evaluation, the longitudinal cross-section J/ψ photoproduction has been neglected since the decay angular distribution in the data is in agreement with the $(1+\cos^2\theta)$ form one

expects for transversely polarised photons, where θ is the decay muon angle respect to the lab direction axis in the J/ψ rest frame.

The observed Q^2 dependence and fitted t dependence can be used to calculate $\frac{d\sigma}{dt}$ at $Q^2 = 0$ and $t = 0$. Fig.13 show this plotted as a function of ν for EMC, BFP and previous photoproduction experiments (6,7,8,9). The decay branching ratio of the J/ψ into muons was taken to be 7 %. The increase with energy observed in the low energy photoproduction measurements is seen to be much less rapid above $\nu = 50$ GeV.

In EMC, the data are consistent with a constant $\frac{d\sigma}{dt})_o^{\text{nucleon}} = 52 \pm 5$ nb/GeV^2. Taking this $\frac{d\sigma}{dt})_o$ and the J/ψ leptonic width and its mass form ref.10 one derives via the optical theorem and the VDM :

$$\frac{d\sigma}{dt})_o (J/\psi N \to J/\psi N) = 82 \pm 20 \ \mu b/GeV^2$$

and $$\sigma(J/\psi N)_{total} = 1.26 \pm 0.31 \text{ mb.}$$

Here any real part in the forward scattering amplitude for elastic $J/\psi N$ scattering is neglected.

b) Inelastic production.

On this topic, we will present the first results obtained by EMC (11). These are based on 126 ± 14 inelastic J/ψ events which are about one half of the whole J/ψ sample (304 ± 22 events). Fig.14 shows the Z dependence of inelastic events. The contribution from ψ',χ and other charmonia higher mass states with subsequent decay into J/ψ account for 40 % of the whole inelastic signal (11 and references therein).

The $p_\perp^2$ distribution (fig.15) shows, as in the elastic case, a coherent and an incoherent part but this last one decreases more slowly : the fit to an exponential form for $p_\perp^2 > .25(GeV/c)^2$ gives a slope parameter $(.85 \pm .13)(GeV/c)^{-2}$.

The Q^2 distribution (fig.16) gives, as best fit to the VDM form, $M = 1.8 \pm 0.2$ GeV, indicating a less steep decrease with Q^2 than for the elastic distribution.

Fig.17 show the ν dependence of the cross-section compared to the photon-gluon fusion model predictions (18). There is good agreement for elastics and also for inelastics below 100 GeV. The data rises sharply above the model at higher ν which can be due to hard gluon emission by $c\bar{c}$ pairs. Elastic and inelastic cross-sections are approximately equal.

c) Study of J/ψ polarisation.

For the results reported up to now the polarisation of the virtual photon and that of the J/ψ has been assumed to be always transverse, in agreement with the data corrected for acceptance being compatible with $(1+\cos^2\theta)$ decay angular fistribution. A more detailed study has been made by BFP dividing the J/ψ sample in 3 bins of Q^2 (fig.18). For low Q^2 and medium Q^2 there is compatibility with $(1+\cos^2\theta)$ whereas high Q^2 rather goes as $(1-\cos^2\theta)$. This means that the longitudinal cross-section is rising with Q^2. In fig.19 the a coefficients found for $1+a\cos^2\theta$ are plotted versus Q^2 and compared to different values of $R_\psi = \frac{\sigma_L}{\sigma_T}$. From VDM for lighter vector mesons, one would expect $R_\psi = \frac{Q^2}{2M_\psi^2}$ but this doesn't seen to be the behaviour of the data nor $R_\psi = 0$ (completely transverse polarisation). A form $R_\psi = \frac{4Q^2}{M_\psi^2}$ is closer to the data.

Now if the longitudinal cross-section is not negligible, it becomes meaningless to fit the Q^2 dependence to a single parameter M in a form $(1+\frac{Q^2}{M^2})$. In fig.21 the BFP analysis gives $M = 3.25\pm0.45$ GeV when one assumes $\frac{\partial}{\partial Q^2}(\sigma_L/\sigma_T) = 0$ but $M = 1.65\pm0.10$ GeV when one assumes $\sigma_L/\sigma_T = \frac{Q^2}{2\varepsilon}$ and takes $\varepsilon * \frac{eff_L}{eff_T} \sim 1$ to extract the Q^2-dependence of σ_T where eff_L and eff_T are the detection efficiencies for longitudinal and transverse polarisations.

5. OPEN CHARM PRODUCTION.

a) EMC two-muon events (ref.15).

To select a clean sample of dimuons events, one must mainly deal in EMC experiment with the fact that a third muon could have escaped detection. So from a starting sample containing all events with two reconstructed muon tracks, the detectors in the beam can be used to veto on the events where the third muon remains in the beam region. Punch-through hadrons are rejected by asking the interaction vertex to be in the upstream part of the target. Fig.22 show the $(\mu^+\mu^-)$ and $(\mu^+\mu^-)$ missing energy plots before and after these cuts. The $(\mu^+\mu^-)$ sample still contains (fig.22c) events where the third muon cannot be seen by the detectors in the beam. Events with $E_{missing} > 90$ GeV are then rejected since the two parts of the plot are clearly separated and we are left with 344 events $(\mu^+\mu^-)$ and 401 events $(\mu^+\mu^-)$.

Other cuts are than applied to keep only events in a kinematic region where the acceptance is smooth : $E_{\mu_1} > 20$ GeV, $\theta_{\mu_1} > 7$ mrad, $E_{\mu_2} > 16$ GeV, $y = \frac{\nu}{E} < 0.91$, $Q^2 > 1$ GeV^2 where 2 refers to the scattered and 2 to the secondary muon.

The cross-sections computed after acceptance corrections are seen to be equal for $(\mu^+\mu^-)$ and $(\mu^+\mu^-)$ within statistical errors in each kinematic bin. So in the following, the two will be added.

The data have been compared to a QCD model for charm production (12). In this model a $c\bar{c}$ pair is produced by proton gluon fusion (fig.4b). This model is used as input into the Monte Carlo with a gluon momentum distribution $G(\eta) = \eta^{-1}(1-\eta)^5$ where η is the fraction of the nucleon momentum carried by the interacting gluon and a coupling constant $\alpha_S(Q^2) = 12\pi/27 \log(Q^2/\Lambda^2)^2$ where $\Lambda = 0.5$ GeV.

Extra assumptions must be made for the C quark to D meson fragmentation function and for the charmed quark mass. These are simply $D(Z_c) = \delta(Z_c - 1)$ and $m_c = m_D$.

D mesons are then assumed to decay in $K_{\mu\nu}$ or $K^*_{\mu\nu}$ with equal probabilities and a branching ratio $(D \rightarrow \mu)$ of 10 % is taken. In fig.23 data are compared to this model. Q^2, W, Z and

$p_\perp^2$ distributions are shown and also in each case the estimated background from π or K decay is drawn.

The model describes well the data both in shape and normalisation. The agreement at low Z can certainly be improved by a better fragmentation function whereas the excess of events at high Z is probably due to background coming from tridents with one muon of very low momentum escaping both the spectrometer and the beal detectors.

The mean missing energy in this (2μ) sample is about 20 GeV giving extra support to the charm hypothesis since the expect missing energy for π,K decay is about 8.5 GeV.

b) BFP Dimuon events.

This experiment has a much larger statistics since about 20000 events with (2μ) in final state are left after apparatus cuts. 81 ± 10 % of these are estimated to be charm, the rest being π,K decay. Cuts for smooth acceptance are applied, namely vertex position, $E_{hadr} > 36$ GeV, $E_{\mu_2} > 15$ GeV, $\nu > 75$ GeV, $p_\perp$ of $\mu_2/\mu_1 > 0.45$ GeV.

Preliminar results of the analysis (13) show that the photon-gluon model describes reasonably well the data in ν, Q^2, Z. E missing and p respect to γ_v distributions. The input parameters into the model for the comparison are $M_C = 1.5$ GeV, $G(\eta) = 3(1-\eta)^5\eta^{-1}$, $D(Z_C) = (1-Z_C)^{0.4}$, fraction of μ'S/$c\bar{c}$ pair = 0.199 with $C \to D \to K_{\mu\nu}$(61 %) or $C \to D \to K^*_{\mu\nu}$(39 %).

Calculation of the total (but in the forward direction) cross-section gives :

$$\sigma_{forward}\ (\mu N \to \mu c\bar{c}X) = 6.9\ ^{+1.9}_{-1.4}\ nb$$

to be compared to the Michigan State University (14) results at 275 GeV : 3 ± 1 nb.

From that and extrapolating at $Q^2 = 0$:

$\sigma_{forward}\ (\gamma N \to c\bar{c}X) = 750\ ^{+180}_{-130}$ nb at $\langle\nu\rangle = 178$ GeV

$\sigma_{forward}\ (\gamma N \to c\bar{c}X) = 560\ ^{+200}_{-100}$ nb at $\langle\nu\rangle = 100$ GeV

Charm photoproduction is thus seen to rise with energy. However charm is only a small part of $\sigma_T(\gamma N)$.

These results can also be presented under the form of structure functions for charm instead of cross-sections. If F_2^{CHARM} is defined as :

$$F_2(\mu N \to \mu c\bar{c}X) = \frac{d^2\sigma}{dQ^2 d\nu} \cdot \frac{Q^4 \nu}{(1-y+\frac{y^2}{2})} \cdot \frac{1}{4\pi\alpha^2}$$

this function is seen to be, as expected, violently scaling non-invariant. One can then estimate the amount of the observed scaling violations in muon-nucleon scattering which are due to charm and this is seen to give a 30 % contribution on scaling violations of F_2(all) for $Q^2 < 10$. All muon data in this range are sensitive to that.

c) EMC Trimuon events (ref.16).

To explore the sources for trimuon events, let us look at fig.24-25 where $M_{\mu^+\mu^-}$ for 3μ events has been plotted for elastic and inelastic events respectively. In both cases vertex and momentum cuts have already been applied (p>10 GeV for all muons). The QED trident Monte Carlo calculation is indicated in the figures as a dashed curve. Elastic events nicely follow this curve, except in the J/ψ mass peak and for $M_{\mu^+\mu^-} \leq 1$ GeV where the acceptance calculation for tridents is uncertain and where other contributions like ρ decay can be present.

On the other hand the inelastic events are clearly in excess over QED tridents. To study the other contributing processes, the mass region $1 \leq M_{\mu^+\mu^-} \leq 2.5$ GeV is selected to get rid of both the J/ψ contribution and the uncertainties in acceptance at low mass.

Since the main contribution to the inelastic QED events comes from bremstrahlung, the method to separate them from the events in excess over QED uses the STAC[(a)] information on the shower-shape to discriminate between electromagnetic and hadronic showers. The separation can be done event by

(a) Sample Total Absorption Calorimeter is the name of the heavy target in EMC Experiment. The deposited hadronic energy will be named E_{STAC}.

event for $E_{STAC} > 80$ GeV and also on a statistical basis defining a hadronic probability for $20 < E_{STAC} < 80$ GeV. Rejecting the events with $E_{STAC} < 20$ GeV where the separation is not possible, we are left with 122 events (75 after weighting by hadronic probability). Fig.26 show their Z distribution. A contribution of inelastically produced QED events (different from the elastic + bremstrahlung events already substracted) is still present and can be removed by retaining only events with $Z < 0.6$ which are in clear excess over the QED background. Then we are left with 60 events (42 after weighting).

These events have not only large hadronic energy but also large missing energy as seen from the 20 events out of the 60 where the 3 muons are fully reconstructed in the spectrometer (not with the detectors in the beam) and all three momenta are then measured. It is found $\langle E_{mis} \rangle = 43$ GeV to be compared to $\langle E_{mis} \rangle = 7.7$ GeV for the J/ψ events.

These events are compared to the γg fusion model for charm production (fig.27). Again as in the 2μ case, the model is used as input into a Monte Carlo which simulates all steps of the detection in the apparatus and all conditions of the reconstruction program and the output is compared to the data. To deal only with smooth acceptance regions a cut $X_{Feynman} > 0$ was applied. The model parameters were the same as in the (2μ) case.

The data are well represented by this model in all 4 variables : ν, q^2, Z, p^2. Also shown is the contribution from hadrons (π, K) decay. It is seen to be < 10 % in all kinematic regions and the missing energy would be about 12 GeV.

Other backgrounds have been estimated and none was found to explain the signal :

-Production of $\rho'(1250)$, $\rho'(1550)$ < 4 %
-Residual QED events with $Z < 0.6$ < 5 %
-Tail of inelastic ρ < 10 %

An interesting process, other than charm production, would be Drell-Yan pairs. However this is estimated to be only 10 to 20 % of the observed signal and in the process no missing energy is expected.

6. OTHER INTERESTING PROCESSES.

Coming back to the processes listed in 2c), the following results have been reached by the different experiments.

a) T Production (BCDMS).

From the 24 events observed in $8\ \text{GeV} \leq M_{\mu^+\mu^-} \leq 12\ \text{GeV}$ and comparison with the QED expectations, a 90 % confidence limit can be set (17) : $\sigma_T * \text{B.R.}(T \to \mu^+\mu^-) \leq 6\times10^{-39}\text{cm}^2/\text{nucleon}$.

b) M° or M^{++} Heavy lepton (BFP).

From the high $p_\perp$ events in their dimuon sample, $\sigma_M * \text{B.R.}(M \to \mu\mu\mu) \leq 10^{-35}\text{cm}^2$ (3) for M_M between 3 and 12 GeV (fig.20).

c) $B\bar{B}$ Production (BFP).

9 events with 5μ and 9 events with 4μ are observed. One (4μ) events is likely to be (ref. 3 for detailed arguments).

$$\mu N \to \mu N + \begin{cases} B \to C\mu^-\nu\mu \\ \bar{B} \to \psi X, \quad \psi \to \mu^+\mu^- \end{cases}$$

Presence of $b\bar{b}$ production in the (2μ) or (3μ) sample is being investigated by this experiment.

CONCLUSIONS.

Elastic J/ψ production by muons has been seen to have a Q^2 dependence well described by VDM with a propagator mass close to $M_{J/\psi}$.

However this is only valid with the restriction that the longitudinal cross-section is rising with Q^2. The differential cross-section $\left(\frac{d\sigma}{dt}\right)_{t=o}$ increase rather slowly with the photon energy above 50 GeV.

Inelastic J/ψ cross-section is approximately equal to the elastic one and 5 times larger than the ψ' contribution. It increases rapidly with the photon energy.

Two-muon events production on Fe targets is seen to be mainly charm ($D\bar{D}$) production. Three-muon events are mostly electromagnetic tridents with an excess of inelastic events due to charm. As well for (2μ) as for (3μ) the data are well

described by the QCD photon-gluon fusion model for charm production.

Acknowledgements.

I am indebted to all my colleagues in EMC and particularly to C.Best, J.K.Davies, C.Goessling and T.Sloan for the many discussions and explanations on the multimuon results. I want also to thank J.J.Aubert for his comments on the preparation of this lecture.

I am very grateful to the organisers of the International Winter Meeting for fundamental physics for the very pleasant stay in Ronda.

TABLE 1

	BFP	EMC	BCDMS
Laboratory	FNAL	CERN	CERN
Beam (μ^+)	209 Gev	280 GeV	280 GeV
Intensity/s	1.5 to 6×10^6	$\sim 2 \times 10^7$	$\sim 2 \times 10^7$
Target Length	Fe 5 Kg/cm^2	Fe 1.5 kg/cm^2	C 8 Kg/cm^2
Flux (μ^+) Luminosity	8×10^{10} 2.5×10^{38}	8×10^{10} 0.75×10^{38}	1.5×10^{11} 7.5×10^{38}
% of Data	$\sim$ 20 %	$\sim$ 20 %	$\sim$ 20 %
μ Detection	Spectrometer fully sensitive in beam region	Spectrometer + Prop. Chambers and hodoscope in beam	Spectrometer + End Detector
Calorimeter target Resolution $\frac{\Delta E_{nad}}{E_{nad}}$	$1.5 * E^{-0.5}$	$0.55 * E^{-0.4}$	

TABLE 2

TOPICS COVERED BY EACH EXPERIMENT

J/ψ Production	Measured Cross Section	BFP, EMC, BCDMS
	$Q^2, \nu, t(Z)$ dependences	Elastics : BFP, EMC Inelastics : EMC
	J/ψ Polarisation σ_L, σ_T Separation	BFP

Open Charm Production	Measured Cross-Section	BFP
	Q^2, ν, Z, p^2 Dependences	2 muons : BFP, EMC 3 muons : EMC

REFERENCES.

1) J.Gayler, Contribution to this Conference.
2) G.Smadja, Contribution to this Conference.
3) A.R.Clark et al., Invited paper presented at the International Symposium on Lepton and Photon Interactions at High Energies, FNAL, Aug.1979.
4) A.R.Clark et al., "Observation of J/ψ (3100) production by 209 GeV muons", Physical Reviex Letters, 43,187 (July 1979).
5) J.J.Aubert et al., "Measurement of J/ψ production in 280 GeV/c μ^+ Iron Interactions", Physics Letters 89B, 267 (January 1980).
6) B.Knapp et al., Physical Review Letters 34,1040 (1975).
7) U.Camerini et al., Physical Review Letters 35,483(1975).
8) T.Nash et al., Physical Review Letters 36,1233 (1975).
9) B.Gittelman et al., Physical Review Letters 36,1616(1975).
10) A.M.Boyarski et al., Physical Review Letters 34,1357(1975).
11) European Muon Collaboration, "Inelastic J/ψ production in 280 GeV/c muon Iron Interactions", to be published.
12) Leveille et Weiler, Nuclear Physics B147, 147 (1979).
13) M.Strovink, Presentation at Les Arcs Conference (1980).
14) D.Bauer et al., Physical Review Letters 43,1551 (1979).
15) European Muon Collaboration, "Dimuon production in muon iron interactions", to be published.
16) European Muon Collaboration, "Trimuon production in 280 GeV/c muon iron interactions", to be published.
17) A.C.Benvenutti, Contribution to the International Symposium on Lepton and Photon interactions at high energies, FNAL, Aug. 1979.
18) T.Weiler, Physical Review Letters 44, 304 (1980).

FIGURES.

1) Definition of measurable quantities in (3μ) events.
2) Definition of kinematic variables.
3) Sources of multimuon events (backgrounds).
4) Sources of multimuon events (interesting processes).
5) Sources of multimuon events (other interesting).
6) Invariant mass $(\mu^+\mu^-)$ in BCDMS Experiment.
7) Invariant mass $(\mu^+\mu^-)$ in EMC Experiment.
8) Invariant mass $(\mu^+\mu^-)$ in BFP Experiment.
9) t distribution of elastic J/ψ events (EMC).
10) t distribution of elastic J/ψ events (BFP).
11) Q^2 dependence (EMC).
12) Q^2 dependence (BFP).
13) ν dependence of $\left(\frac{d\sigma}{dt}\right)_{t=o}$.
14) Z dependence of inelastic J/ψ events (EMC).
15) $p_\perp$ dependence of inelastic J/ψ events (EMC).
16) Q^2 dependence of inelastic J/ψ production (EMC).
17) ν dependence of J/ψ cross-section (EMC).
18) Decay angular distributions in different regions of Q^2(BFP)
19) Longitudinal to transverse cross-section ratio versus Q^2(BFP)
20) Limits for M° or M^{++} cross-section (BFP).
21) Q^2 dependence of transverse cross-section (BFP).
22) Missing energy of dimuon events (EMC).
23) Dimuon events distributions (EMC).
24) $M_{\mu^+\mu^-}$ for elastic trimuon events (EMC).
25) $M_{\mu^+\mu^-}$ for inelastic trimuon events (EMC).
26) Z distribution for hadronic trimuon events (EMC).
27) Trimuon events distribution (EMC).

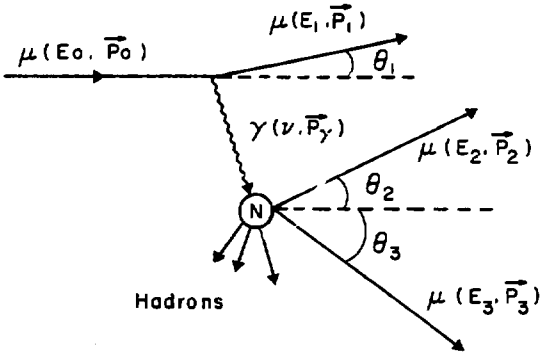

Fig. 1 - Definition of Measurable Quantities in (3μ) Events

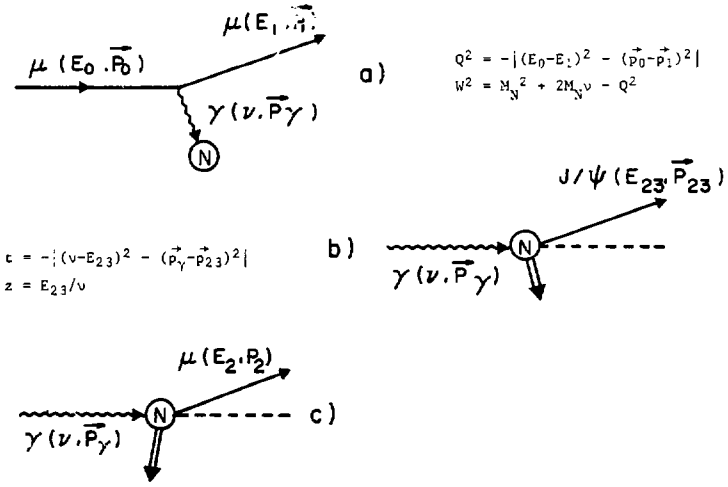

Fig. 2 - Definition of Kinematic Variables

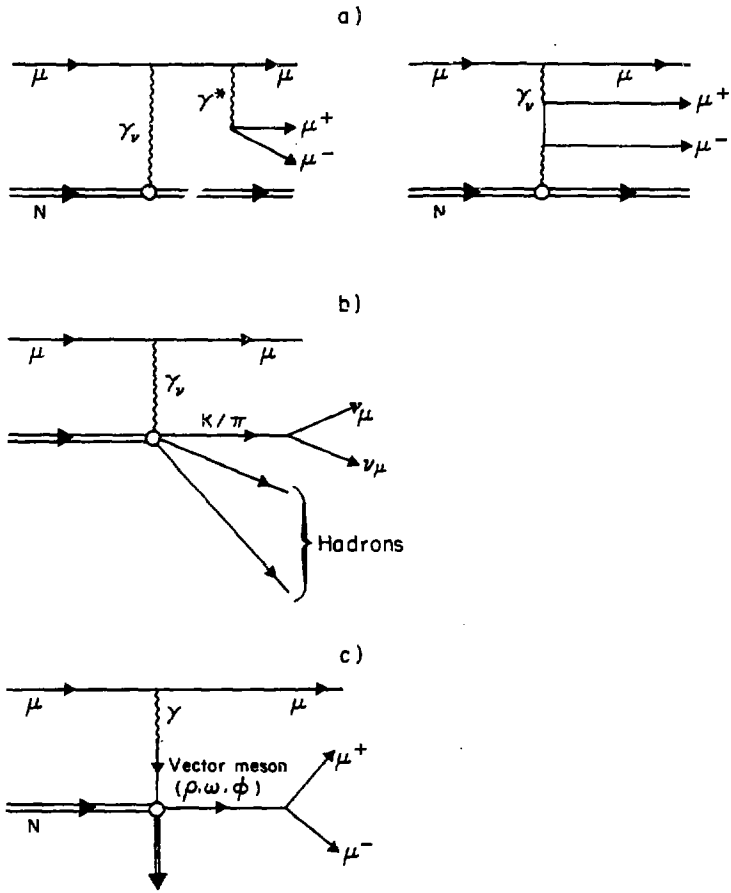

Fig. 3 - Sources of Multimuon Events (Backgrounds)

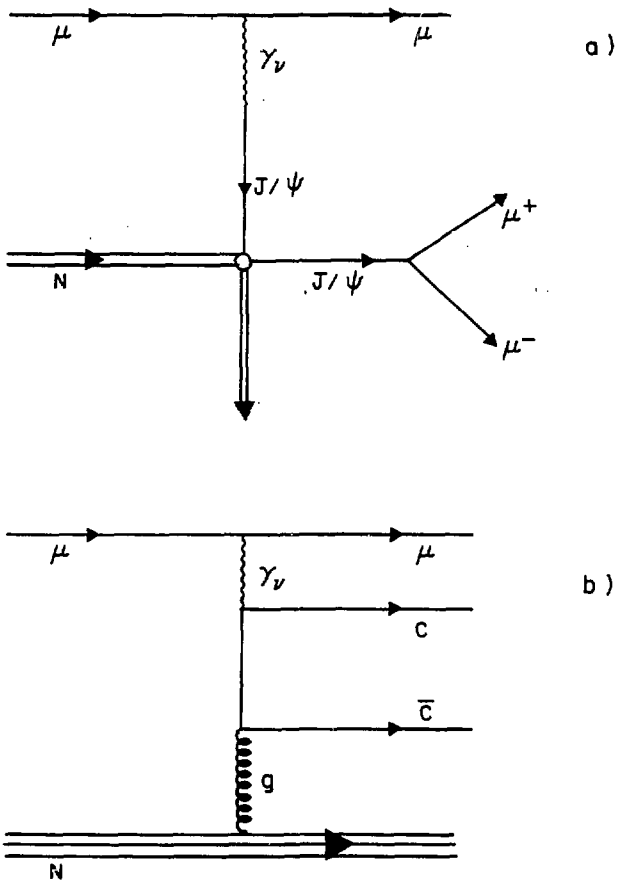

Fig. 4 - Sources of Multimuon Events (Interesting processes)

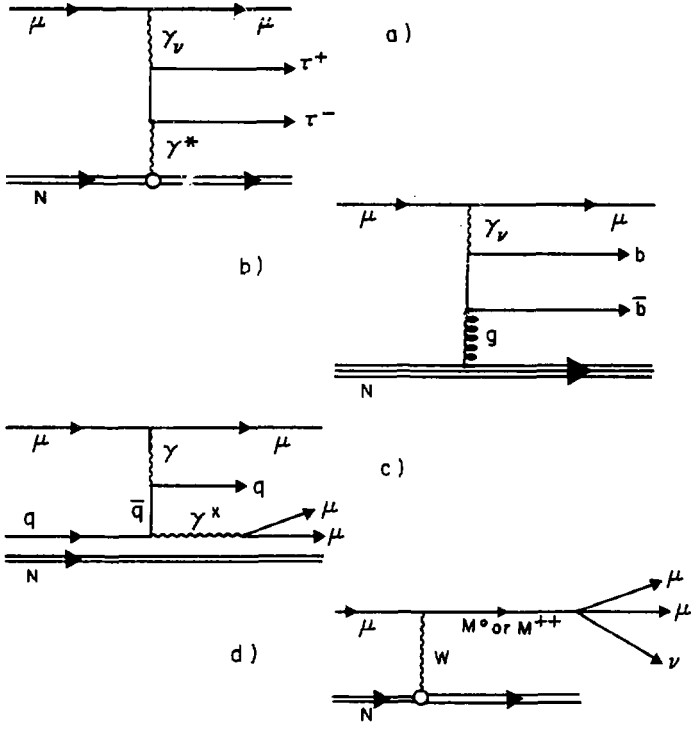

Fig. 5 - Sources of Multimuon Events (Rare processes)

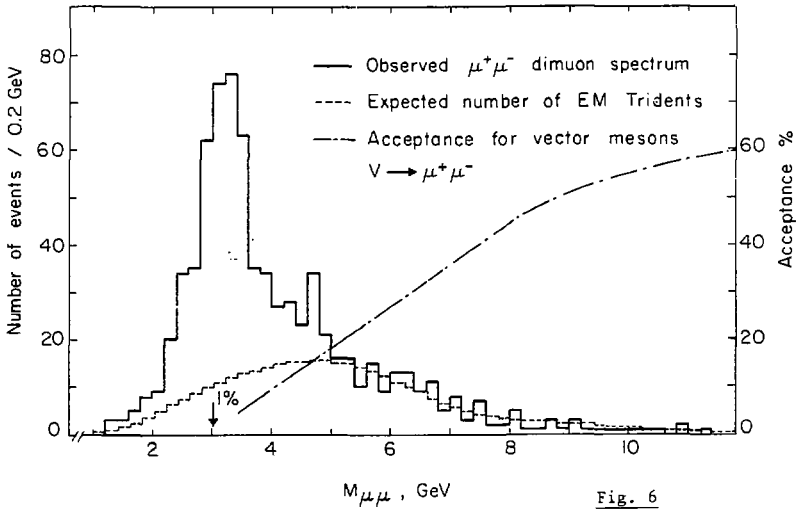

Fig. 6

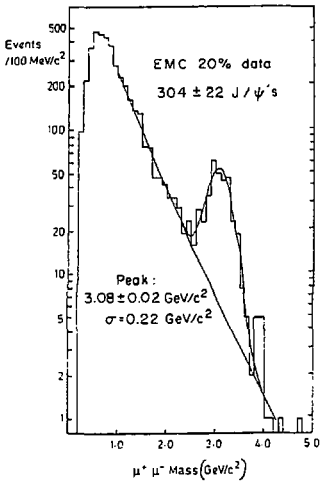

Fig. 7

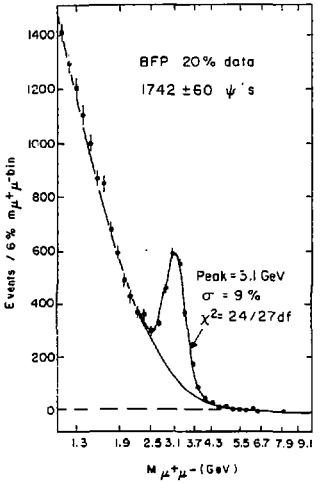

Fig. 8

Fig. 6 to 8 - Invariante Mass ($\mu^+\mu^-$)

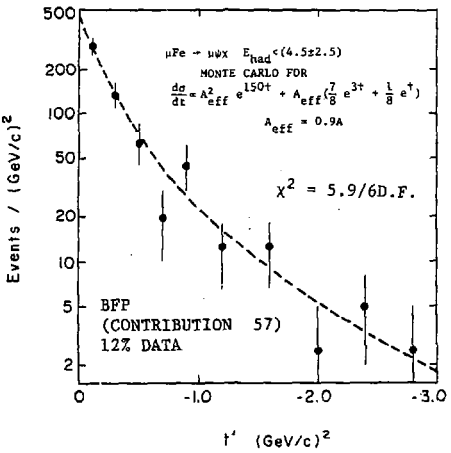

Fig. 9 - t Distribution of Elastic J/ψ Events (EMC)

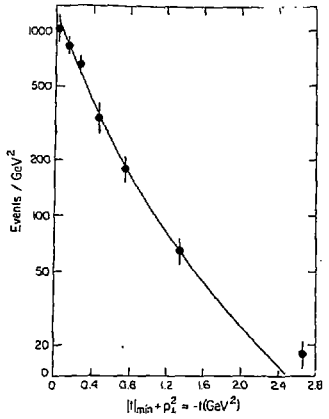

Fig. 10 - t Distribution of Elast J/ψ Events (BFP)

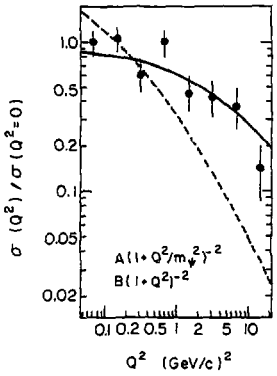

Fig. 11 - Q^2 Dependence (EMC)

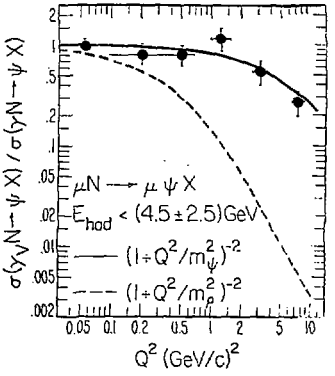

Fig. 12 - Q^2 Dependence (BFP)

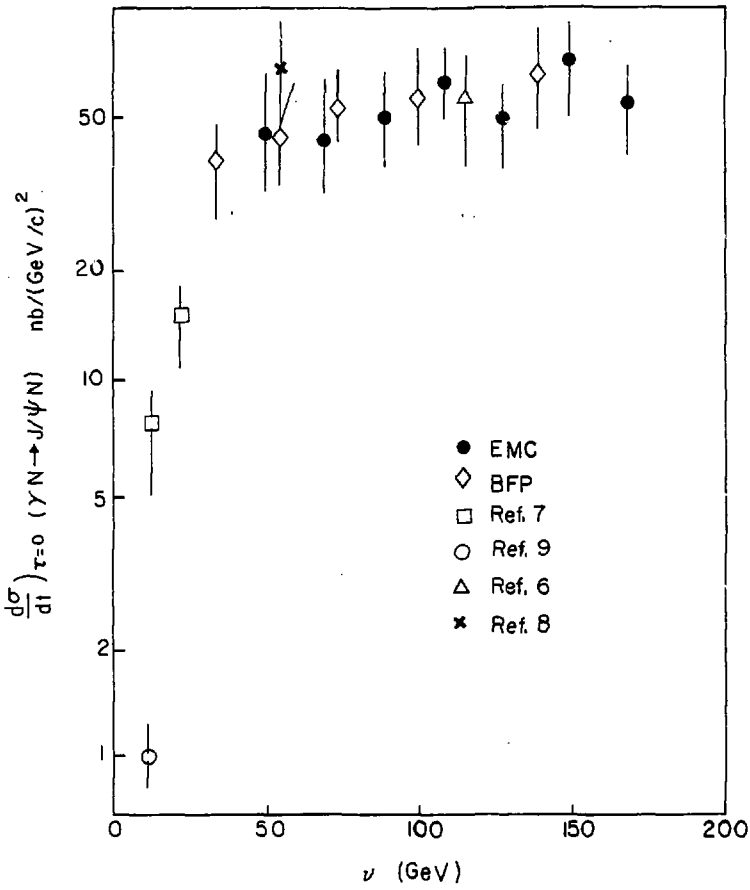

Fig. 13 - ν Dependence of $\frac{d\sigma}{dt}\Big)_{t=0}$

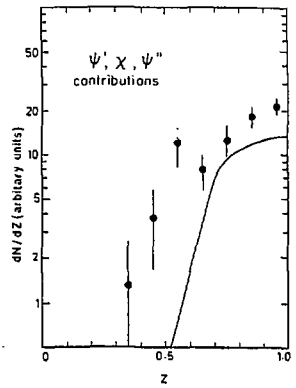

Fig. 14 - z Dependence of Inelastic J/ψ Events (EMC)

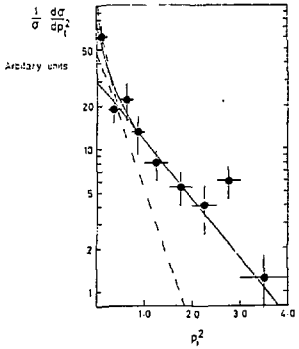

Fig. 15 - p_t^2 Dependence of Inelastic J/ψ Events (EMC)

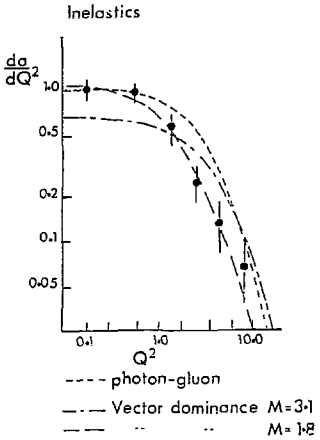

Fig. 16 - Q^2 Dependence of Inelastic J/ψ Events (EMC)

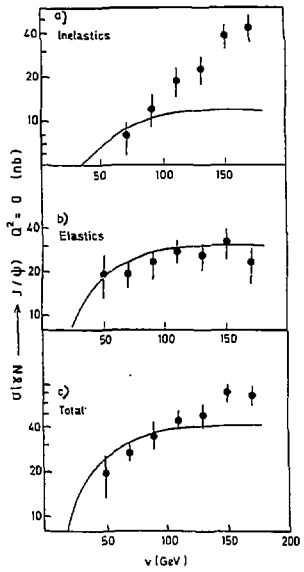

Fig. 17 - ν Dependence of J/ψ Cross-section (EMC)

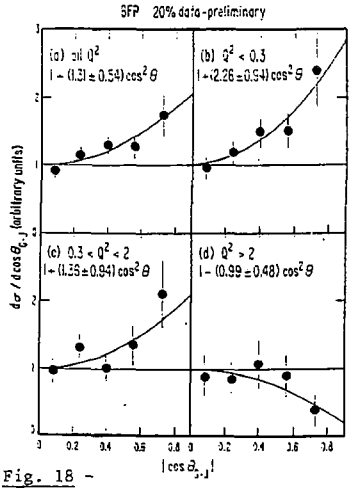

Fig. 18 - Decay Angular Distributions in Different Regions of Q^2 (BFP)

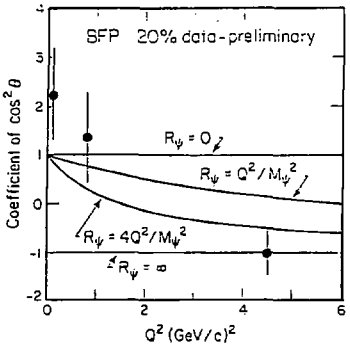

Fig. 19 - Q^2 Dependence of Longitudinal to Transverse Cross-section Ratio (BFP)

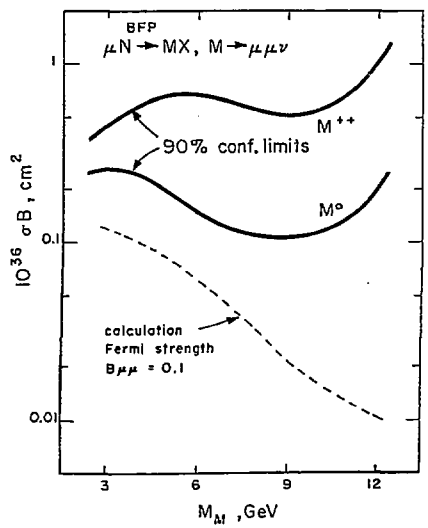

Fig. 20 - Limits for M^0 or M^{++} Cross-section (BFP)

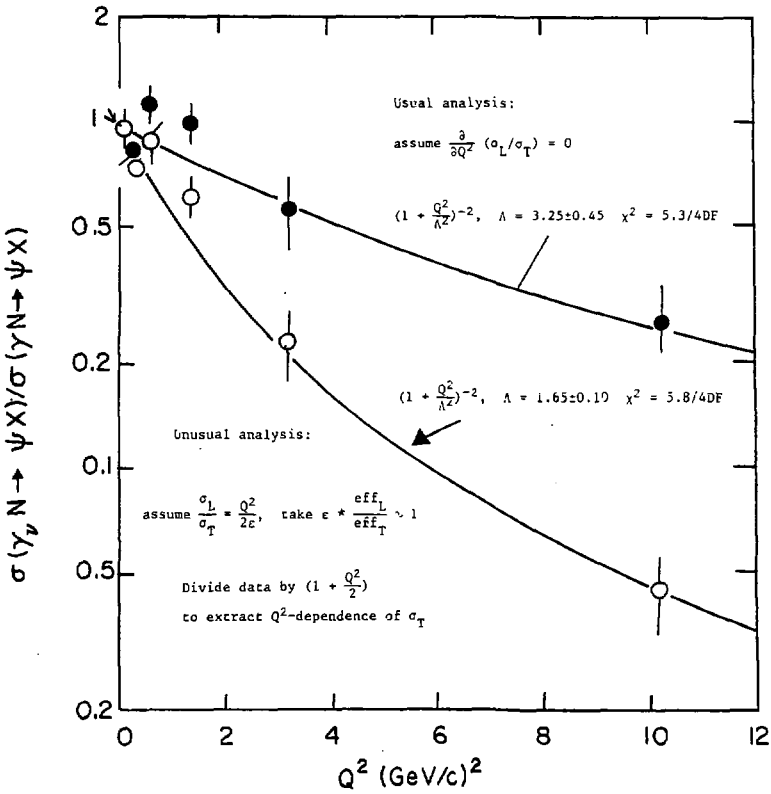

Fig. 21 - Q^2 Dependence of Transverse Cross-section (BFP)

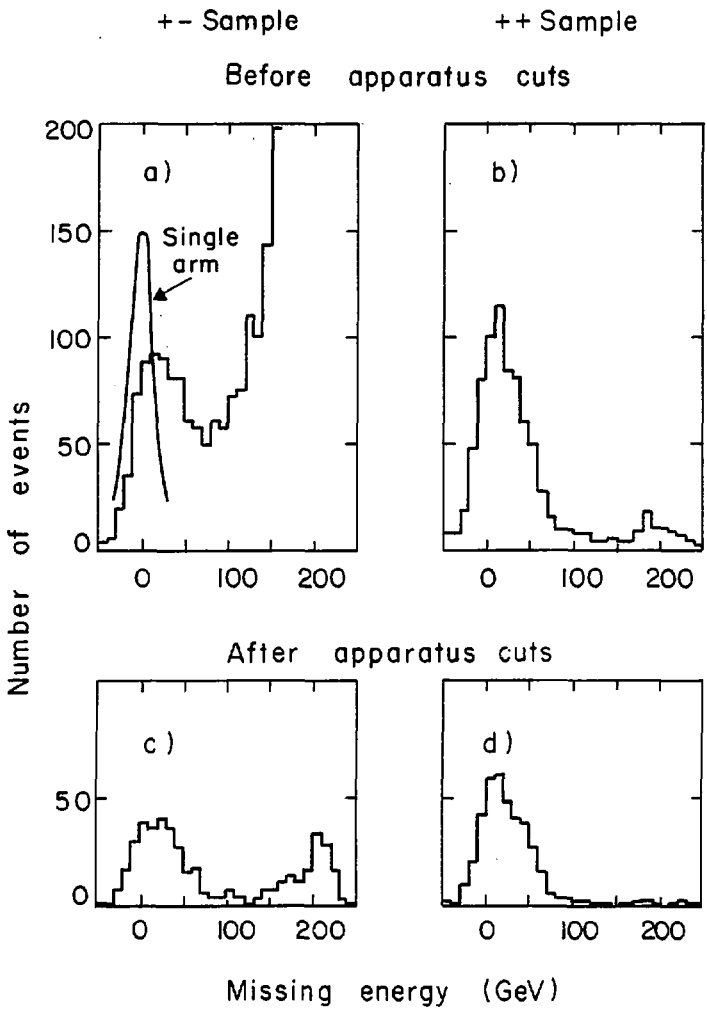

Fig. 22 - Missing Energy of Dimuon Events (EMC)

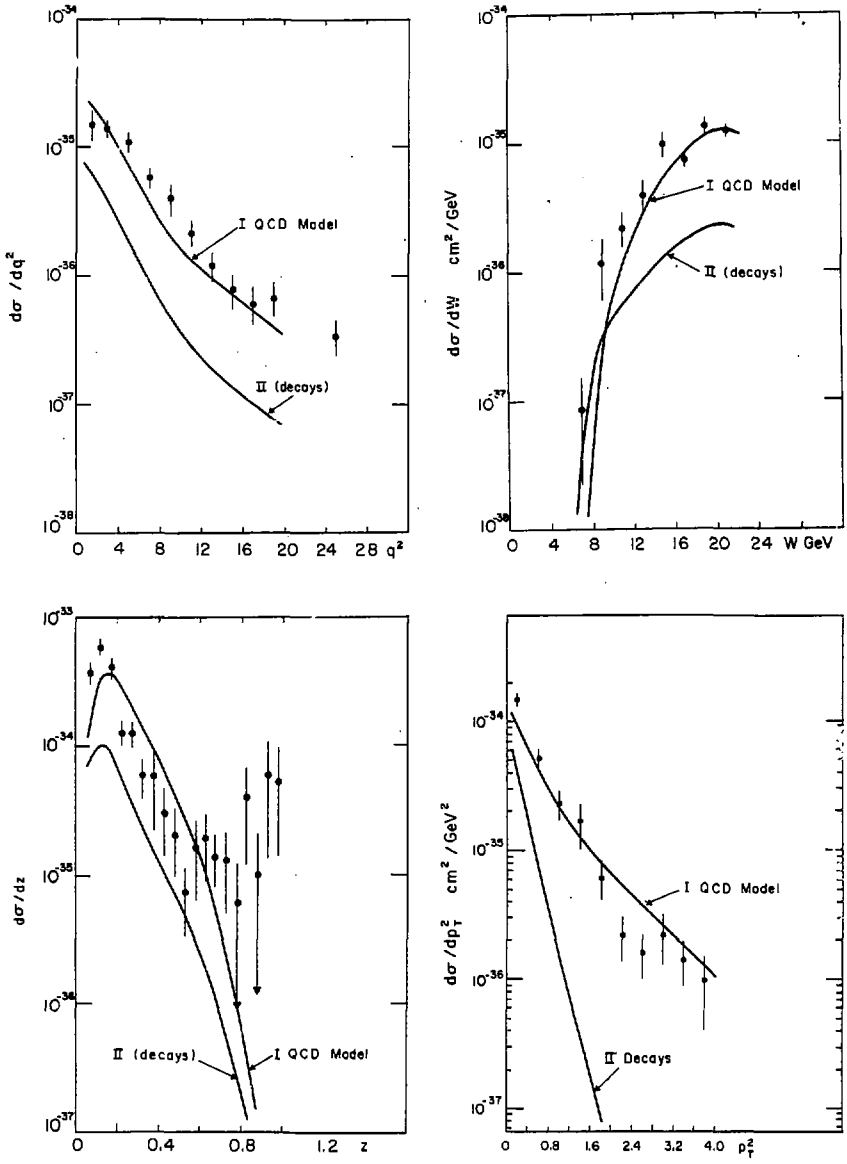

Fig. 23 - Dimuon Events Distributions (EMC)

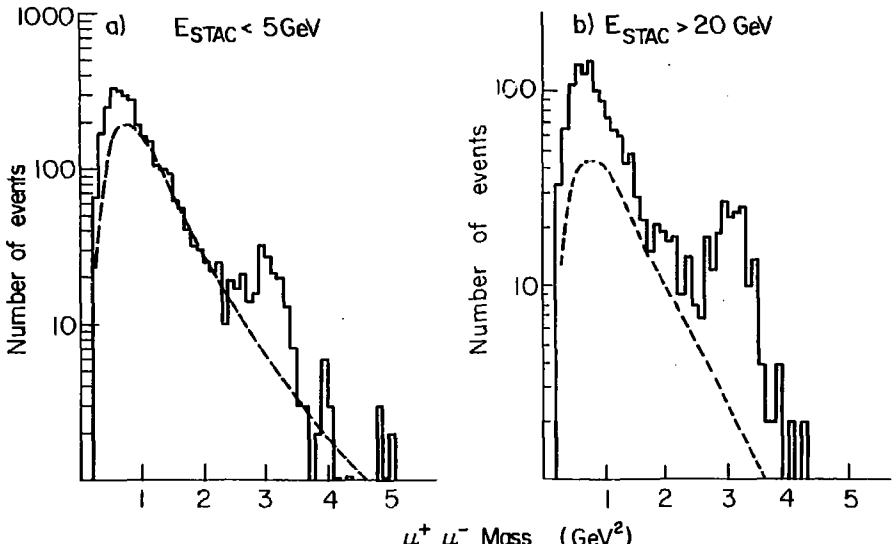

Fig.24 : M $\mu^+\mu^-$ for elastc trimuon events (EMC)

Fig.25 : M $\mu^+\mu^-$ for inelastic trimuon events (EMC)

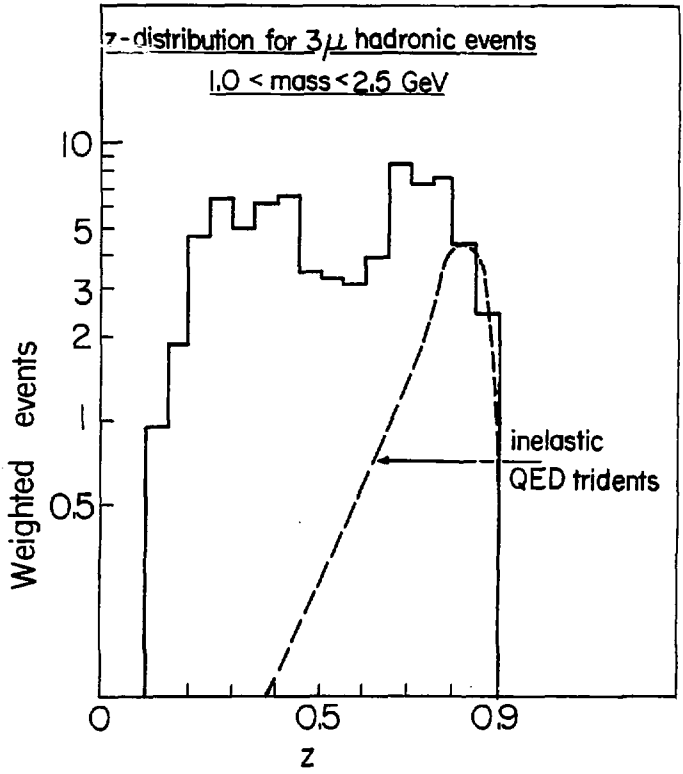

Fig. 26 - z Distribution for Hadronic Trimuon Events (EMC)

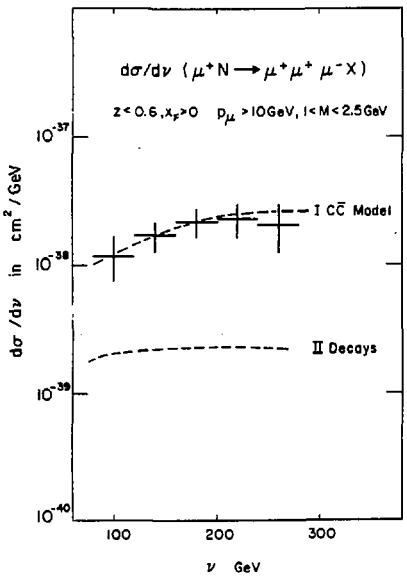

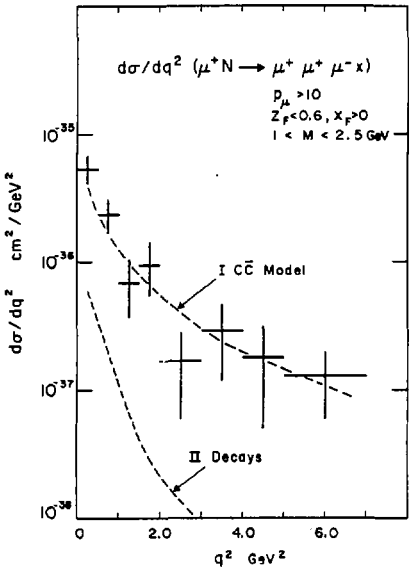

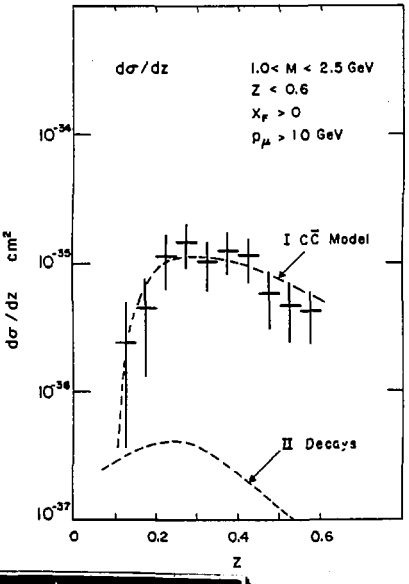

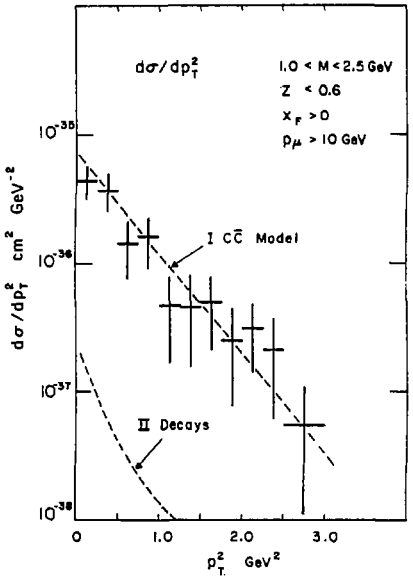

Fig. 27 - Trimuon Events Distributions (EMC)